Ruth Olmer | Lena Engels | Abdulai Usman | Sandra Menke | Muhammad Nasir Hayat Malik | Frank Pessler | Gudrun Göhring | Dorothee Bornhorst | Svenja Bolten | Salim Abdelilah-Seyfried | Thomas Scheper | Henning Kempf | Robert Zweigerdt | Ulrich Martin

Differentiation of Human Pluripotent Stem Cells into Functional Endothelial Cells in Scalable Suspension Culture

Suggested citation referring to the original publication:
Stem Cell Reports 10 (2017) 5,
DOI https://doi.org/10.1016/j.stemcr.2018.03.017
ISSN 2213-6711

Stem Cell Reports
Resource
OPEN ACCESS

Differentiation of Human Pluripotent Stem Cells into Functional Endothelial Cells in Scalable Suspension Culture

Ruth Olmer,[1,2,3,11] Lena Engels,[1,2,11] Abdulai Usman,[1,2,3] Sandra Menke,[1,2,3] Muhammad Nasir Hayat Malik,[4,9,10] Frank Pessler,[4,9,10] Gudrun Göhring,[5] Dorothee Bornhorst,[2,6] Svenja Bolten,[2,7] Salim Abdelilah-Seyfried,[6,7] Thomas Scheper,[2,8] Henning Kempf,[1,2] Robert Zweigerdt,[1,2] and Ulrich Martin[1,2,3,*]

[1]Leibniz Research Laboratories for Biotechnology and Artificial Organs (LEBAO), Department of Cardiothoracic, Transplantation and Vascular Surgery (HTTG), Hannover Medical School, Carl-Neuberg-Str.1, 30625 Hannover, Germany
[2]REBIRTH-Cluster of Excellence, Hannover Medical School, 30625 Hannover, Germany
[3]Biomedical Research in Endstage and Obstructive Lung Disease Hannover (BREATH), German Center for Lung Research (DZL), 30625 Hannover, Germany
[4]TWINCORE Centre for Experimental and Clinical Infection Research, 30625 Hannover, Germany
[5]Institute of Cell and Molecular Pathology, Hannover Medical School, 30625 Hannover, Germany
[6]Institute of Molecular Biology, Hannover Medical School, 30625 Hannover, Germany
[7]Institute of Biochemistry and Biology, Potsdam University, Karl-Liebknecht-Straße 24-25, 14476 Potsdam, Germany
[8]Institute for Technical Chemistry, Leibniz University Hannover, 30167 Hannover, Germany
[9]Helmholtz-Centre for Infection Research Braunschweig, 38124 Braunschweig, Germany
[10]Centre for Individualised Infection Medicine, 30625 Hannover, Germany
[11]Co-first author
*Correspondence: martin.ulrich@mh-hannover.de
https://doi.org/10.1016/j.stemcr.2018.03.017

SUMMARY

Endothelial cells (ECs) are involved in a variety of cellular responses. As multifunctional components of vascular structures, endothelial (progenitor) cells have been utilized in cellular therapies and are required as an important cellular component of engineered tissue constructs and *in vitro* disease models. Although primary ECs from different sources are readily isolated and expanded, cell quantity and quality in terms of functionality and karyotype stability is limited. ECs derived from human induced pluripotent stem cells (hiPSCs) represent an alternative and potentially superior cell source, but traditional culture approaches and 2D differentiation protocols hardly allow for production of large cell numbers. Aiming at the production of ECs, we have developed a robust approach for efficient endothelial differentiation of hiPSCs in scalable suspension culture. The established protocol results in relevant numbers of ECs for regenerative approaches and industrial applications that show *in vitro* proliferation capacity and a high degree of chromosomal stability.

INTRODUCTION

Endothelial cells (ECs) are crucial for vascular homeostasis and interact with circulating cells as well as neighboring cells present in the vessel walls. They are involved in thrombosis and platelet adhesion, immune and inflammatory responses, and the modulation of vascular tone and blood flow (Esper et al., 2006; Michiels, 2003). Disturbances in endothelial function are connected to a large variety of pathologic processes such as atherosclerosis, congestive heart failure, or pulmonary hypertension (Esper et al., 2006; Sakao et al., 2009), to name just a few.

Hence, ECs were also used in many *in vitro* disease models to investigate vascular dysfunction, for instance with regard to diabetes and atherosclerosis progression (Goya et al., 2003), coronary artery disease (Farcas et al., 2009), or to investigate influenza A virus (IAV) infection (Hiyoshi et al., 2015). ECs from different sources have also been utilized as cellular therapeutics in a multitude of experimental concepts (e.g., Franck et al., 2013; Tang et al., 2011). Primary ECs were utilized for vascular tissue engineering approaches either to seed human tissue-engineered blood vessels (L'Heureux et al., 2006) or for the re-endothelialization of biological vascularized matrix (Andrée et al., 2014). Moreover, ECs were used to improve hematocompatibility of titanium nanostructures (Mohan et al., 2013) as well as gas-exchange membranes for extracorporal oxygenation (Hess et al., 2010). EPCs were already applied in a variety of clinical trials for the therapy of pulmonary hypertension or limb ischemia (Chong et al., 2016). In another approach, endothelialization of acellularized heart valves directly from the blood stream *in situ* after implantation resulted in fully hematocompatible functional valves with growth potential (Cebotari et al., 2011; Theodoridis et al., 2015), which underlines the therapeutic potential. ECs and EPCs therefore represent key cell types for the investigation of the pathogenesis of human disease, for drug screening, conduction of safety studies, cellular therapies, or for *in vitro* engineering of all kinds of vascularized tissue.

As yet, various sources of ECs were utilized for experimental *in vitro* and *in vivo* studies, and for therapeutic applications. For *in vitro* studies on endothelial biology immortalized EC lines with features of aortic, venous, or microvascular phenotype are still frequently used, e.g., for modeling the blood-brain barrier (Cucullo et al., 2008;

Daniels et al., 2013) or angiogenesis (Heiss et al., 2015; Shao and Guo, 2004). Such cell lines have clear advantages, in particular the unlimited potential for proliferation and the straightforward cell culture, but their similarity to primary ECs is limited (Boerma et al., 2006). Immortalized cell lines are generally not useful for *in vivo* studies because of their tumorigenic potential. For experimental purposes, neonatal ECs can be isolated from cord blood (human cord blood ECs [hCBECs]) or from umbilical veins (human umbilical vein ECs [hUVECs]). As neonatal cells, hUVECs show relatively high proliferation capacities and are frequently used experimentally. However, although hUVECs are widely used in transplantation models (e.g., Matrigel plug assays [Kang et al., 2009; Skovseth et al., 2002]), not in all cases did the cells show the expected functional features (Orlova et al., 2014). ECs and EPCs from adult individuals, which would be required for autologous cell therapies, can be isolated from different sources including peripheral blood. However, while the commonly used "early outgrowth" EPCs are *de facto* mainly monocytes (Gruh et al., 2006; Rohde et al., 2006; Zhang et al., 2006), the so-called "late outgrowth" EPCs, also called endothelial colony-forming cells, represent ECs grown from circulating EPCs or ECs (Bou Khzam et al., 2015; Colombo et al., 2013). One important limitation of these cells, however, is the donor-dependent substantial variation in isolation efficiency, as well as the very limited expandability (Igreja et al., 2008), especially in case of elderly donors. Further sources for primary ECs comprise surplus saphena vein fragments from bypass surgery or adipose tissue available from plastic surgery.

For the majority of therapeutic applications, at least 0.3×10^9 ECs would be required, as recently estimated based on cell numbers that have been applied in rodent models (Asahara et al., 2011; Corselli et al., 2008). Although expansion of hUVECs or hCBECs in conventional 2D EC culture is laborious and hardly allows for clinical scale-up, the production of such cell numbers ($\sim$30 population doublings $\hat{=}\sim$ passage 5) is in principle possible. However, it is unlikely that the resulting cells could meet the clinical requirements, not least because the high frequencies of chromosomal aberrations that have been observed in primary ECs represent a potential drawback for experimental research and a substantial risk for cellular therapies (Corselli et al., 2008; Johnson et al., 1992; Nichols et al., 1987). Chromosomal abnormalities are not necessarily connected with impaired cellular function or tumor growth, and can be observed in healthy somatic tissue types such as the liver (Mayshar et al., 2010; Shuga et al., 2010). On the other hand, 90% of all human solid tumors are aneuploid (Albertson et al., 2003), and many tumors are associated with chromosomal abnormalities. Thus ECs carrying chromosomal abnormalities may not only show impaired or altered cell function but may also give rise to tumor formation.

ECs derived from human pluripotent stem cells (hPSCs), with their unlimited expansion potential, are considered as an alternative cell source for experimental studies, tissue engineering, and, especially, therapeutic approaches (Kim and von Recum, 2008; Reed et al., 2013). In contrast to the cell sources discussed above, they promise to combine two important features: (1) a theoretically unlimited availability as derivatives of hPSCs and (2) the availability as an autologous cell source for transplantation purposes. Already in 2002 Levenberg et al. (Levenberg et al., 2002) could successfully generate ECs from human embryonic stem cells (hESCs). Since then a variety of differentiation protocols were established to generate ECs from hPSCs mainly applying sequential addition of growth factors such as BMP4 and vascular endothelial growth factor A (VEGFA) in embryoid body-based cultures. These approaches yielded between 2% (Levenberg et al., 2002) and 15% of $CD31^{pos}$ (Rufaihah et al., 2011) cells. Modulation of the WNT pathway in combination with BMP4 in these cultures resulted in 25% to >40% of $CD31^{pos}$ cells (Tan et al., 2013; Yang et al., 2008). More defined differentiation conditions based on monolayer cultures and combined addition of growth factors and small molecules (e.g., WNT activation and cAMP elevating agents) resulted in 20%–81% of $CD31^{pos}$ cells (Ikuno et al., 2017; Lian et al., 2014; Liu et al., 2016; Orlova et al., 2014; Patsch et al., 2015; Yamamizu and Yamashita, 2011). Orlova et al. (2014) demonstrated that iPSC-derived ECs performed significantly better in a vascular plexus model *in vitro* but also in an organotypic transplantation model *in vivo* in zebrafish compared with the widely used hUVECs.

Although substantial progress has already been achieved concerning reproducibility and the utilization of defined and prospectively guanosine monophosphate good manufacturing practice (GMP)-compliant conditions, the robust generation of large numbers of hPSC-derived ECs for industrial applications and cellular therapies is still a major hurdle. Although expansion of undifferentiated hPSCs in controllable, stirred-tank bioreactors (Kropp et al., 2016; Olmer et al., 2012), and further differentiation toward cardiomyocytes (Kempf et al., 2014) is reality by now, published 2D endothelial differentiation protocols are barely scalable.

Addressing this current limitation, we now demonstrate the efficient and robust generation of ECs from hPSCs in scalable suspension cultures applying a straightforward three-step differentiation protocol. The generated ECs show all typical features of ECs and maintain their functional properties during prolonged culture for at least ten passages. Moreover, a high degree of karyotype stability was observed during culture expansion.

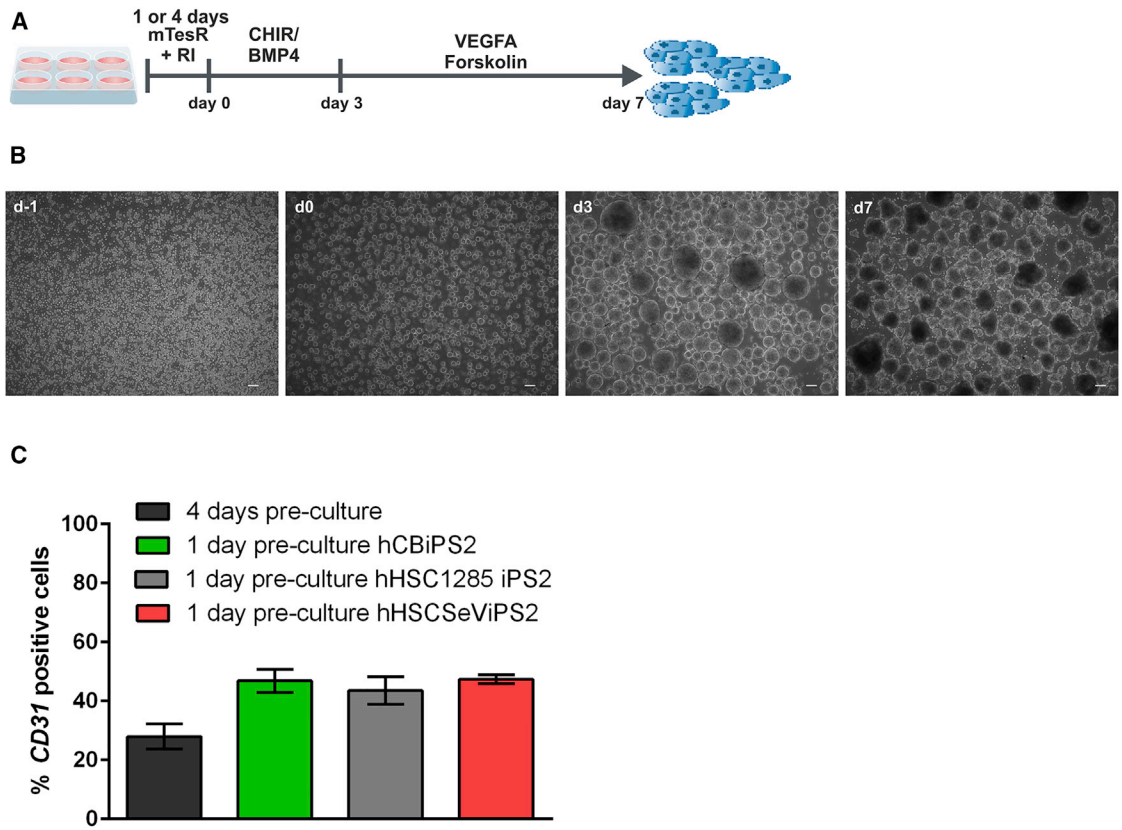

Figure 1. EC Differentiation in Small-Scale Static Suspension Cultures

hiPSC differentiation toward endothelial cells was performed according to the scheme depicted in (A). Cells were cultured in six-well suspension plates either 4 days or 1 day prior to initiation of differentiation conditions. Cell-only aggregates develop on day 1 and increase in size during differentiation (B). Scale bars, 100 μm. Flow cytometric analysis on day 7 of differentiation showed 27.86% ± 4.1% (combined data from hCBiPS2, hHSC1285iPS2, and hHSCSeViPS2; n = 15 independent experiments; mean ± SEM) *CD31*^{pos} cells after 4 days of pre-culture and 46.9% ± 3.9% (hCBiPS2; n = 3 independent experiments; mean ± SEM) *CD31*^{pos} cells and 43.5% ± 4.5% (hHSC1285iPS2; n = 3 independent experiments; mean ± SEM), 47.4% ± 1.4% (hHSCSeViPS2; n = 3 independent experiments; mean ± SEM) *CD31*^{pos} cells, respectively, for three independent cell lines with one day of pre-culture (C). See also Figure S1A.

RESULTS

Generation of *CD31*^{pos} Cells from hiPSCs in Static (Small-Scale) Suspension Cultures

For the differentiation of human induced pluripotent stem cells (hiPSCs) aggregates in suspension culture we adapted a 2D differentiation protocol by Patsch et al. (2015). Starting from single-cell suspension, hiPSCs were grown as floating aggregates in static six-well suspension cultures (Figures 1A and 1B). Differentiation in aggregates toward *CD31*^{pos} cells was induced on day 4 by treatment with an activator of WNT signaling (CHIR 99021) and BMP4 for 3 days followed by VEGFA and forskolin treatment for 4 days (Figure 1A). Analysis of *CD31* expression by flow cytometry on day 7 of differentiation resulted in 27.9% ± 4.2% (hCBiPS2, hHSC1285iPS2, and hHSCSeViPS2; n = 15) of *CD31*^{pos} cells (Figure 1C). Considering the impact of aggregate size on cardiomyocyte differentiation (Kempf et al., 2014, 2015), we tested different average aggregate sizes as formed at different time points of pre-culture for induction of differentiation. In contrast to the induction of differentiation on day 4 after seeding of single-cell suspensions with an average aggregate size of 75 μm, induction of differentiation on day 1 after seeding with an average aggregate size of 40 μm resulted in 46.9% ± 3.9% *CD31*^{pos} cells (hCBiPS2; n = 3), 43.6% ± 4.5% *CD31*^{pos} (hHSC1285iPS2; n = 3), and 47.3% ± 1.4% (hHSCSeViPS2; n = 3) for three independent hiPSC lines, respectively (Figure 1C). During differentiation culture the aggregates further increased in size reaching a diameter of about 125 μm on day 7 after induction of differentiation (Figure 1B).

Gene expression analysis via quantitative real-time PCR during differentiation showed downregulation of

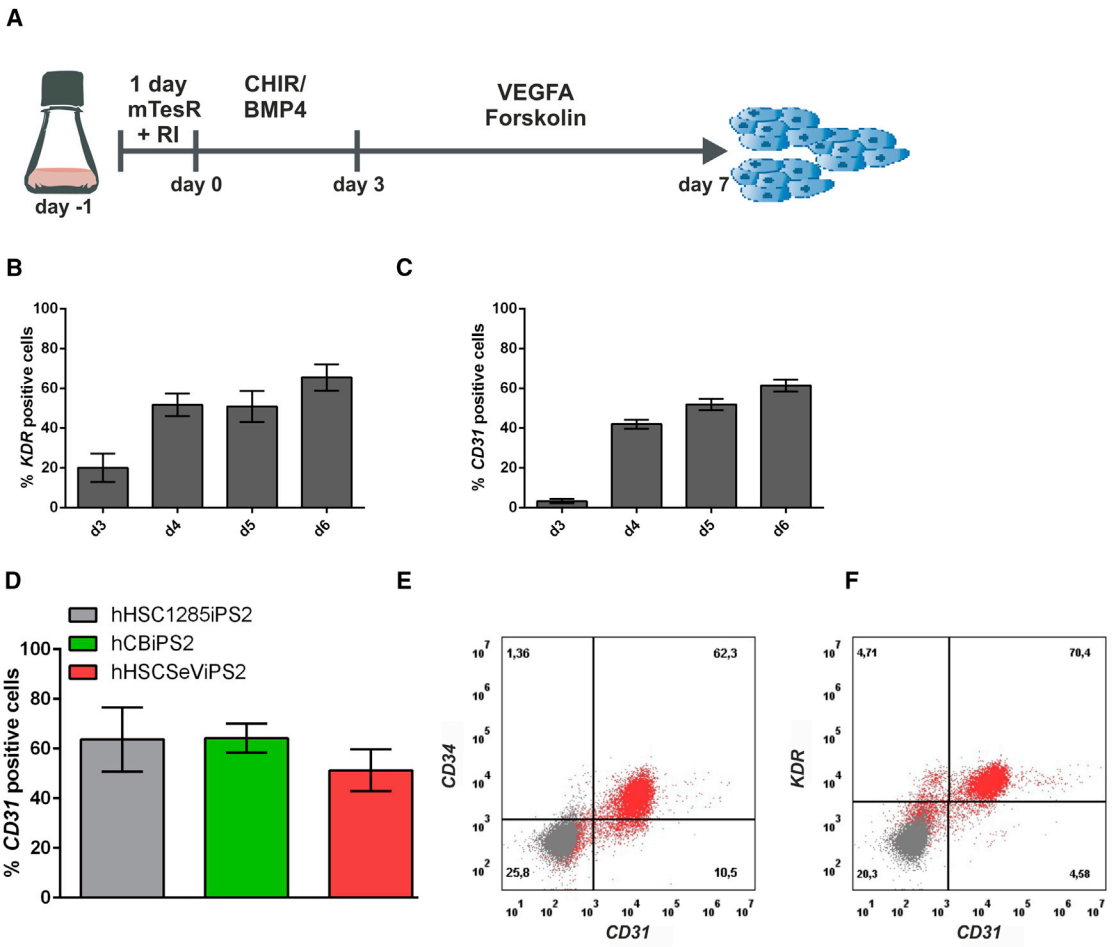

Figure 2. Scale-Up of EC Differentiation to Agitated Erlenmeyer Flasks

hiPSC differentiation toward endothelial cells in agitated Erlenmeyer flasks was performed according to the scheme presented in (A). Flow cytometric analysis showed increase of *KDR* (B) and *CD31* (C) expression from day 3 to 6 onward (n = 6–9 independent experiments, hCBiPS2, hHSC1285iPS2, and hHSCSeViPS2; mean ± SEM). Flow cytometric analysis on day 7 of differentiation revealed for hHSC1285iPS2 63.7% ± 4.9% (n = 7, independent experiments), hCBiPSC2 64.1% ± 2.1% (n = 7, independent experiments), hHSCSeViPS2 49.2% ± 3.3% (n = 8, independent experiments), and *CD31*^{pos} ECs (mean ± SEM) (D). Generated *CD31*^{pos} cells show co-expression of *CD34* (E) and *KDR* (F) (representative plots for hHSCSeViPS2 staining, red; isotype control, gray). See also Figure S1B.

the pluripotency-associated markers *OCT4* and *NANOG* accompanied by upregulation of vascular markers such as vascular endothelial growth factor receptor 2 (*VEGFR2*/*KDR*), *CD31*, and *VEcadherin* (Figure S1A).

Transfer of Differentiation Cultures to Agitated Erlenmeyer Flasks Results in Efficient Generation of *CD31*^{pos} Cells

Based on the promising results of the differentiation experiments in static suspension cultures, we aimed to further optimize the protocol by adaptation to scalable differentiation in agitated Erlenmeyer flasks, as shown in Figure 2A. One day after seeding of single-cell suspensions, the differentiation was initiated by treatment with CHIR99021 and BMP4, and resulted in upregulation of *KDR* from day 3 of differentiation onward, with 65.4% ± 2.6% *KDR*^{pos} cells on day 6 of differentiation (n = 9; hCBiPSC2, hHSC1285iPS2, and hHSCSeViPS2) (Figure 2B). *CD31*^{pos} cells emerged from day 3 onward, reaching 61.4% ± 3.0% *CD31*^{pos} cells on day 6 of differentiation (n = 6; hCBiPSC2, hHSC1285iPS2, and hHSCSeViPS2) (Figure 2C).

During repeated experiments and application of different other hiPSC lines our protocol turned out to be very robust, reproducibly resulting in high differentiation efficiencies. Figure 2D shows typical outcomes for hHSC1285iPS2 with 63.7% ± 4.9% (n = 7), for hCBiPSC2 with 64.1% ± 2.1% (n = 7), and for hHSCSeViPS2 with 49.2% ± 3.3% (n = 8) *CD31*^{pos} ECs, respectively, on day 7

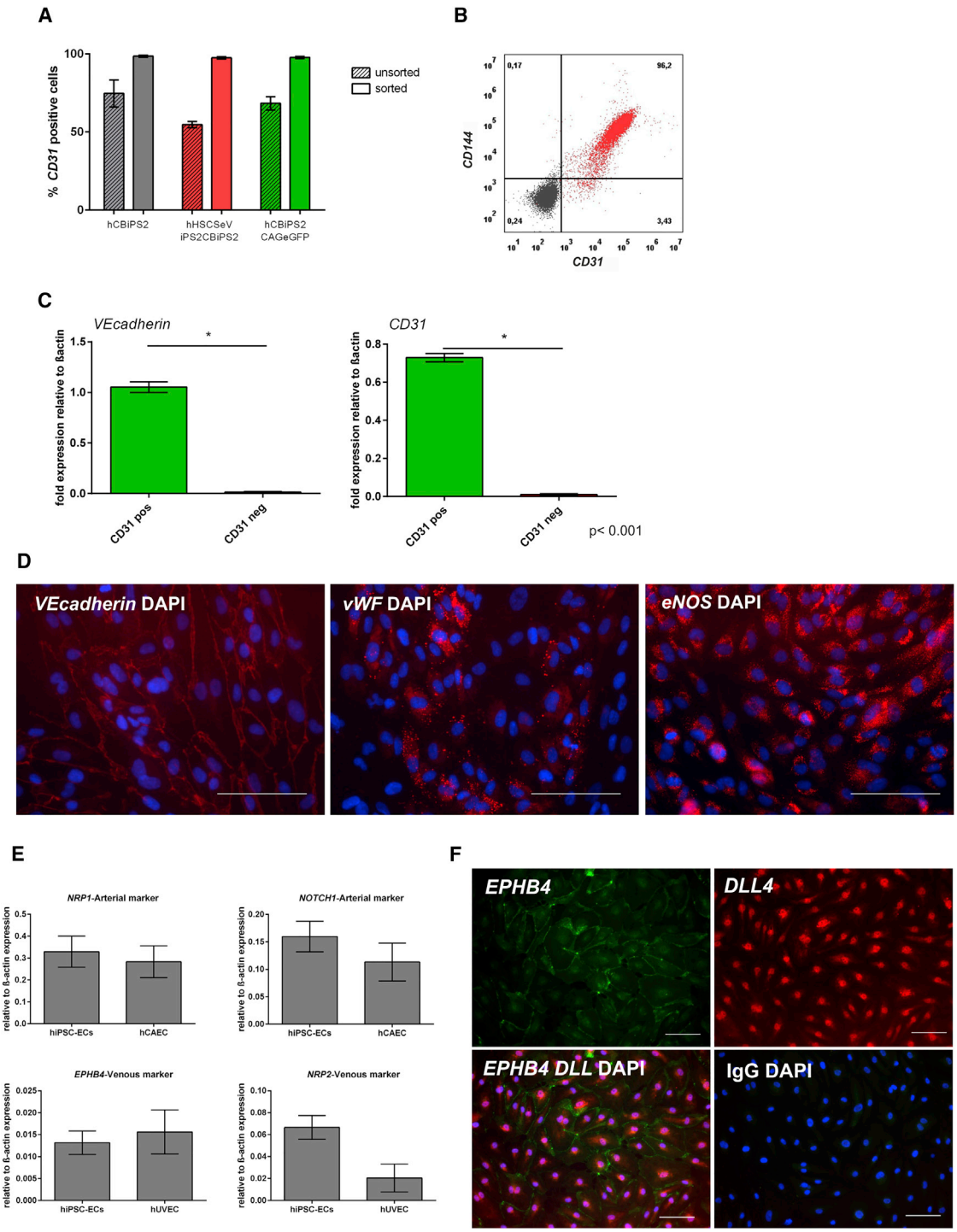

Figure 3. Purified hiPSC-ECs Show Elevated Expression of Typical EC Markers

Flow cytometric analysis resulted in enrichment of *CD31*^{pos} hiPSC-derived ECs from 74.1% ± 8.6% to 98.6% ± 0.5% (hCBiPS2; n = 3), 54.7% ± 2.1% to 97.5% ± 0.7% (hHSCSeViPS2; n = 12), and 68.2% ± 4.1% to 97.8% ± 0.7% (hCBiPS2CAGeGFP; n = 9) *CD31*^{pos} cells (mean ± SEM) by MACS separation (A). Purified *CD31*^{pos} cells showed co-expression of CD144 (*VEcadherin*) (representative plot for hCBiPS2CAGeGFP; staining, red; isotype control, gray) (B). Comparative gene expression analysis showed significant higher *CD31* expression and *VEcadherin* expression in *CD31*^{pos}-sorted hiPSC-ECs compared with the *CD31*^{neg} population (hCBiPS2; n = 3 independent experiments; mean ± SEM, *p < 0.05) (C). Immunocytological stainings for endothelial markers showed homogeneous expression of

(legend continued on next page)

of differentiation. The generated *CD31*^{pos} cells showed co-expression of *CD34* as well as *KDR* (Figures 2E and 2F). In total up to 1.18 × 10^7 *CD31*^{pos} cells could be generated in 20-mL Erlenmeyer flask cultures.

Detailed expression analysis via quantitative real-time PCR showed downregulation of pluripotency-associated markers and increased expression of vascular markers similar to static suspension conditions (Figure S1B).

CD31-Based MACS Separation Yields Highly Enriched *CD31* Cells Expressing Typical Markers and Functional Properties of ECs

By applying *CD31*-based magnetic-activated cell sorting (MACS) separation on day 7 of differentiation the proportion of *CD31*^{pos} cells could be increased from 74.7% ± 8.6% to 98.3% ± 1.0% (hCBiPS2; n = 3), 53.7% ± 1.2% to 96.2% ± 1.6% (hHSCSeViPS2; n = 12), and 68.3% ± 4.2% to 97.4% ± 0.7% (hCBiPS2CAGeGFP; n = 9) *CD31*^{pos} cells, which was highly reproducible (Figure 3A). Sorted *CD31*^{pos} cells showed strong co-expression of CD144 (*VEcadherin*) (Figure 3B). Quantitative real-time PCR analysis of sorted populations showed significantly increased *CD31* mRNA expression and significantly increased *VEcadherin* expression in *CD31*^{pos} hiPSC-ECs compared with the *CD31*^{neg} population (Figure 3C). The enriched hiPSC-ECs showed typical EC morphology in culture, and the homogeneous expression of *VEcadherin*, endothelial nitric oxide synthase and von Willebrand factor (vWF) further confirmed the EC phenotype (Figure 3D). Additional quantitative real-time PCR analysis showed expression of markers for both arterial (NRP1 and NOTCH1) and venous (NRP2 and EPHB4) ECs, with no significant differences in the expression levels compared with control cells (human coronary artery ECs for arterial markers and hUVECs for venous markers) (Figure 3E). Immunofluorescence staining showed co-expression of DLL4 (arterial marker) and EPHB4 (venous marker) in hiPSC-EC cultures (Figure 3F).

The functionality of the MACS-enriched hiPSC-ECs in terms of angiogenic potential was assessed in tube-forming assays, demonstrating that seeding of freshly MACS-sorted *CD31*^{pos} cells on Matrigel results in tube formation after 24 hr, although showing less branching compared with hUVECs, which served as positive control (Figure 4A). Furthermore, homogeneous uptake of acetylated low-density lipoprotein (Dil-Ac-LDL) could be detected in the hiPSC-EC cultures directly after MACS separation (Figure 4B). As a further indication for a normal EC phenotype and functionality, we analyzed the response of the purified hiPSC-ECs to viral infections. Since vascular ECs are natural targets of several human viral pathogens, including IAV (Short et al., 2014), we tested whether MACS-sorted hiPSC-ECs would show expected intracellular responses to infection with an IAV (H1N1) field isolate. Actually, applying an MOI of 1 resulted in significant levels of viral hemagglutinin mRNA detected at 12 hr post infection (pi), followed by a sustained increase until 48 hr pi (Figure 4C). This was accompanied by increases in mRNA expression for interferon-γ (IFN-γ), CXCL10, and ISG15, all of which are typically induced in vascular endothelium during IAV infection (Figure 4D). Similar data were obtained from an independent experiment featuring half the infectious dose (MOI = 0.5) (Figures 4C and 4D).

hPSC-Derived ECs Show High Proliferative Potential and Maintain Their Endothelial Phenotype, Functional Properties, and Stable Karyotype after Extended Culture Expansion

After MACS sorting, hiPSC-ECs could be expanded on fibronectin-coated plates in EGM-2 medium for up to 12 passages while retaining their typical EC phenotype and stable *CD31* surface expression up to passage 10 after sorting (Figure 5A). Furthermore, expanded hiPSC-ECs (P10) showed homogeneous expression of *VEcadherin* and *vWF*, underlining maintenance of the EC phenotype after *in vitro* expansion (Figure 5B). Population doubling time remained almost stable during *in vitro* passaging (Figure 5C), in addition clonal proliferation potential is also preserved during passaging (Figure S2). Based on stable expansion rates (Figure S3), and starting with a total yield of 1.18 × 10^7 hiPSC-ECs from a 20 mL differentiation experiment ~5 × 10^9 hiPSC-derived ECs could be generated within 45 days (10 passages).

To explore whether functionality of the iPSC-ECs is maintained during prolonged culture expansion, hiPSCs-ECs in passage 12 were analyzed in tube-forming assays showing formation of vascular network-like structures (Figure 5D). Moreover, late-passage ECs also showed homogeneous uptake of Dil-Ac-LDL, which represents another functional property of ECs (Figure 5E).

Remarkably, in contrast to primary ECs, late passage hiPSC-ECs showed a high degree of karyotype stability with only one detected karyotypic abnormality (p11, hCBiPS2-EC) among ten analyzed hiPSC-EC cultures. In accordance with recent studies, all hCBECs and hUVECs

VEcadherin, vWF, and endothelial nitric oxide synthase (eNOS) in purified hiPSC-EC cultures (in red; DAPI in blue) (D). Scale bars, 100 μm. Quantitative real-time PCR analysis showed expression of markers for arterial (*NRP1* and *NOTCH1*) as well as venous (*NRP2* and *EPHB4*) ECs (hiPSC2, HSCSeViPS2, and hCBiPS2CAGeGFP; n = 3 each, independent experiments; mean ± SEM) (E). Immunocytological stainings showed co-expression of *EPHB4* (venous markers, green) and *DLL4* (arterial marker, red) in hiPSC-EC cultures; DAPI in blue; representative pictures for HSCSeViPS2-ECs (F). Scale bars, 100 μm.

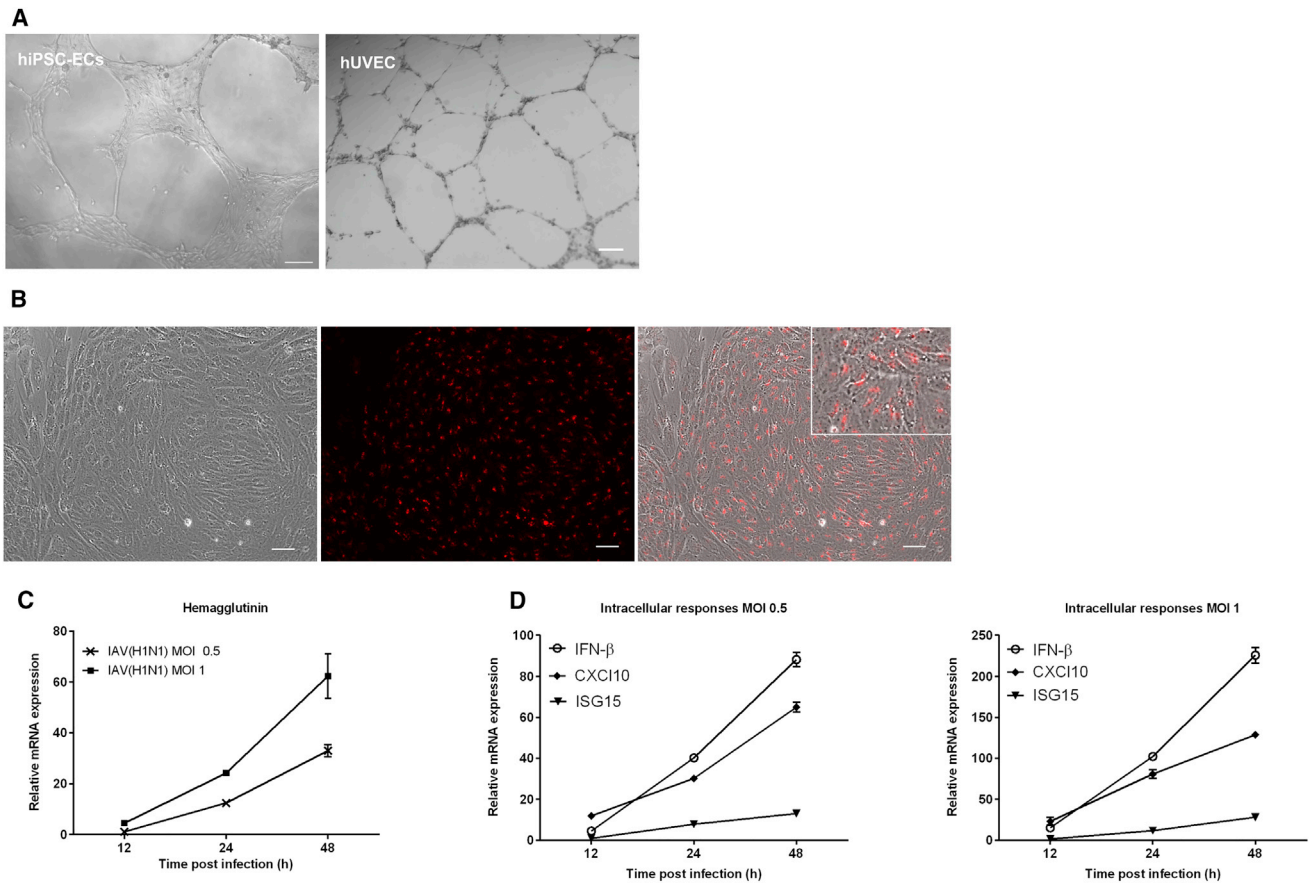

Figure 4. hiPSC-ECs Show a Typical Angiogenic Response in Matrigel and Uptake of Ac-Dil-LDL and Functionally Respond to an IAV Infection

A tube-forming assay demonstrated the angiogenic potential of the hiPSC-ECs comparable with hUVECs (P4 after isolation). Scale bars 100 μm (A). hiPSC-ECs showed uptake of Ac-Dil-LDL after MACS separation (B). Scale bars, 100 μm. Expression analysis showed upregulation of viral hemagglutinin indicating successful infection (C) as well as *ISG15*, *IFN-β*, and *CXCL10* as cellular response (D) after incubation of the cells with IAV (H1N1) for 2 hr with MOI of 0.5 or 1 (hCBiPS2-EC) (n = 3 independent experiments; mean ± SEM).

under similar culture conditions showed karyotype abnormalities in late passages, and a substantial proportion of karyotype abnormalities was observed even in early passages of primary EC cultures from adult donors as well (Figure 5F, listed in Table 1).

To elucidate whether early and late hiPSC-ECs show functional properties *in vivo*, their capacity to integrate into the zebrafish vascular system was evaluated using a xenograft assay (Haldi et al., 2006; Orlova et al., 2014). hiPSC-ECs from early (P1, n = 3) or late (P10/P11, n = 3) passages, as well as early (P1/P4/P5) or late (P14) passages of hUVECs as control cells, were injected into the vasculature at the duct of Cuvier of 48 hr post fertilization zebrafish embryos. After transplantation, hiPSC-ECs and hUVEC-injected zebrafish developed normally; no edema or abnormalities were observed. hiPSC-ECs and hUVECs were observed within the vascular system throughout all regions of the body. No significant differences in integration rates of early passage hiPSC-ECs (61.9%; n = 83/134 embryos) (Figures 6A–6D) and late passage hiPSC-ECs (78.3%; n = 112/143 embryos) could be detected (Figures 6E–6H). In contrast, only 23.5% (n = 32/136 embryos) of the early (P1/P4/P5) passage and 21.6% (n = 23/106 embryos) of the late (P14) passage hUVECs integrated into the zebrafish vascular system (Figure 6I).

Utilization of Fully Controllable Bioreactors Allows for Further Up-Scaling of Differentiation Cultures

To achieve EC numbers which are relevant for therapeutic applications, the established differentiation protocol was transferred to stirred-tank bioreactors with a working volume of 120 mL. As for the smaller Erlenmeyer flasks, cultures were inoculated as single cells. Formed cell aggregates increased in size during differentiation culture (Figure 7A).

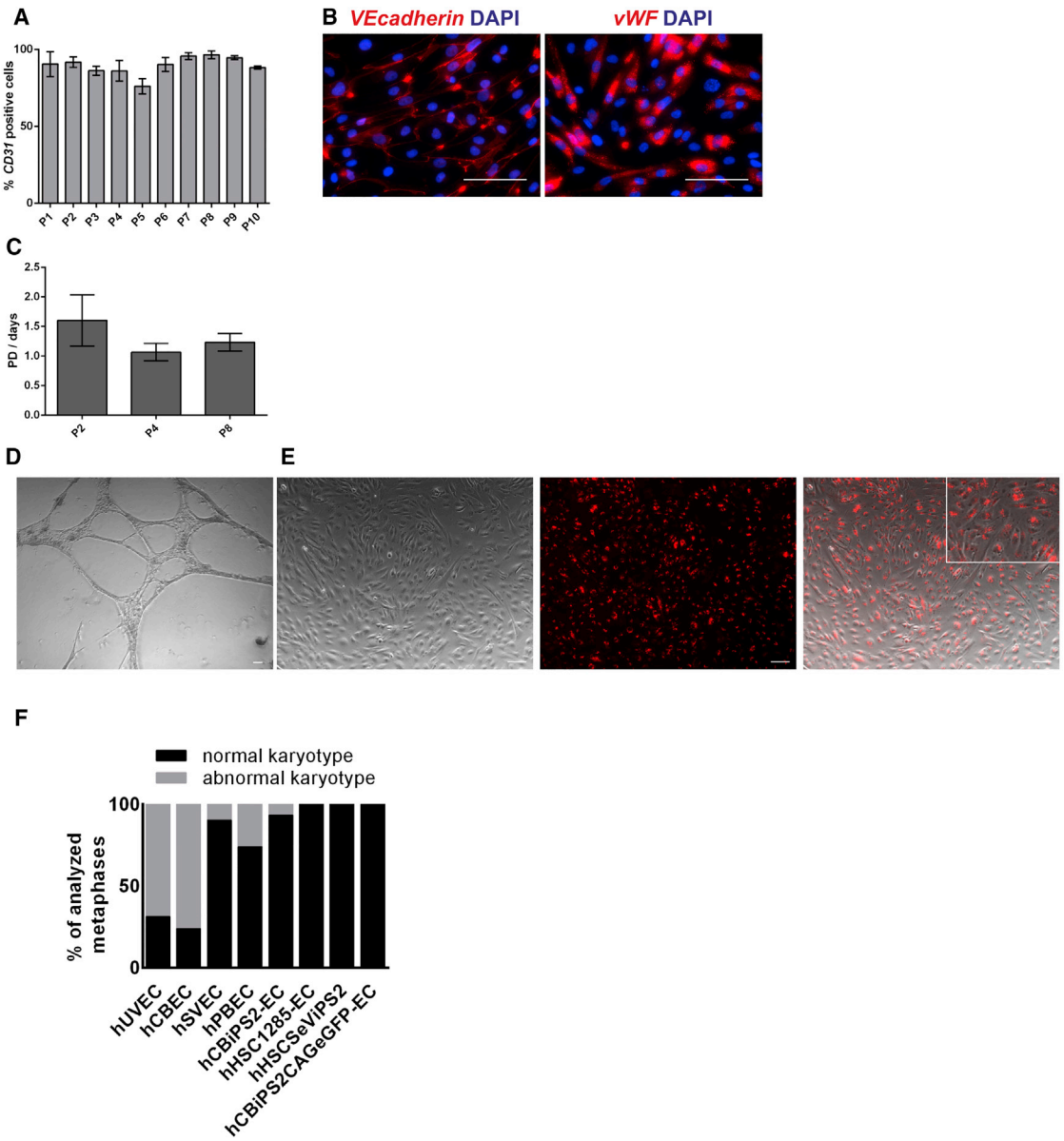

Figure 5. Culture-Expanded hiPSC-Derived ECs Maintain Stable Marker Expression, Proliferation Rates, Cellular Function, and Karyotype

Flow cytometric analysis showed stable expression of *CD31* during *in vitro* passaging for up to 10 passages (n = 3–4 independent experiments; mean ± SEM) (A). Immunocytological stainings for endothelial markers showed homogenous expression of *VEcadherin* and *vWF* in hiPSC-EC cultures after ten passages (in red, DAPI in blue; scale bars represent 100 μm) (B). hiPSC-derived ECs showed stable population doubling time during *in vitro* passaging (n = 3) (C). A tube-forming assay showed angiogenic potential of the generated hiPSC-ECs; scale bars, 100 μm (D). hiPSC-ECs showed unchanged uptake of Ac-Dil-LDL after ten passages of *in vitro* culture. Scale bars, 100 μm (E). Karyotype analyses at passages 11–13 showed frequent karyotype changes in isolated hUVECs as well as hCBECs with abnormalities detected in 68% and 81% of analyzed metaphases, respectively. hSVECs and hPBECs showed abnormalities in 10% of analyzed samples already after up to six passages. Lower frequencies were detected in hiPSC-EC cultures at passages 4–12 with abnormalities in only one cell sample at passage 11 (2% of the analyzed metaphases) (F). See also Figures S2 and S3.

Differentiation initiated after 24 hr resulted in robust generation of 56.8% ± 10.5% $CD31^{pos}$ ECs (hCBiPS2CAGeGFP; n = 3) (Figure 7B). $CD31^{pos}$ cells showed co-expression of *KDR* as well as *VEcadherin* (data not shown). Quantitative real-time PCR analysis showed downregulation of pluripotency-associated markers (*NANOG* and *OCT4*) and

Table 1. Karyotype Analysis of hCBECs, hUVECs, hSVECs, hPBECs, and hiPSC-ECs after *In Vitro* Culture

Sample		Karyotype
Primary ECs		
hUVEC D no. 3	P11	47,XX,+11[7]/94,XXXX,+11,+11[4]/46,XX[5]
hCBEC D no. 22	P13	48,XY,+2,+11[14]
hCBEC D no. 23	P11	91,XXYY,-7[10]/92,XXYY[4]/46,XY[1]
hCBEC D no. 25	P11	47,XY,+i(20) (q10)[5]/91,XXYY,-13[3]/46,XY[8]
hSVEC D no. 31	P5	47,XY,+12[3]/46,XY,del(13)(q21q31)[2]/46,XY[10]
hSVEC D no. 32	P5	46,XX[10]
hSVEC D no. 37	P4	46,XX[10]
hSVEC D no. 38	P4	46,XX[10]
hSVEC D no. 39	P5	46,XX[10]
hSVEC D no. 40	P5	46,XX[10]
hSVEC D no. 41	P5	46,XX[10]
hSVEC D no. 42	P5	46,XX[10]
hSVEC D no. 44	P5	46,XX[10]
hSVEC D no. 47	P5	46,XY,ins(4; 15) (q24; q23q25)[6]/46,XY[4]
hSVEC D no. 49	P6	47,XY,+12[3]/46,XY[16]
hPBEC D no. 37	P3	46,XY,t(X; 2) (q12; p24)[4]/46,XY[11]
iPSC-derived ECs		
hHSC1285-EC	P4	46, XY[15]
hCBiPS2-EC	P8	46, XY [1]
hCBiPS2-EC	P12	46, XY [15]
hCBiPS2-EC	P11	46,XY,add(20) (p12)[2]/46,XY[8]
hHSCSeViPS2-EC	P10	46,XX [12]
hHSCSeViPS2-EC	P10	46, XX [20]
hHSCSeViPS2-EC	P10	46,XX [14]
hCBiPS2CAGeGFP-EC	P10	46,XY[20]
hCBiPS2CAGeGFP-EC	P11	46,XY[20]
hCBiPS2CAGeGFP-EC	P10	46,XY[21]

upregulation of vascular markers such as *KDR*, *CD31*, and *VEcadherin* (Figure 7C). Purified ECs displayed typical EC morphology in culture (Figure 7D), showed uptake of Dil-LDL (Figure 7E) and formed networks on Matrigel (Figure 7F).

The utilized bioreactor system allows for online monitoring of temperature, dissolved oxygen (DO), as well as pH, during culture. While temperature is kept stable DO and pH are decreasing with progressing culture due to metabolic activity and recover with medium exchanges; typical datasets are shown in Figure S4.

DISCUSSION

Technologies for production of patient- and disease-specific ECs on a clinical and industrial scale will be a basic requirement for high-throughput drug screening and EC-based cellular therapies, including engineering of clinically applicable engineered vascularized tissue transplants. Whereas primary EC preparations suffer from several drawbacks including limited potential for expansion and a high likelihood for development of karyotype abnormalities, hiPSCs may provide a superior source for patient-derived ECs, enabling the production of theoretically unlimited cell numbers. Whereas expansion of undifferentiated hiPSCs is already possible in defined media in scalable suspension culture, targeted differentiation of hiPSCs under defined conditions is as yet possible only in hardly scalable 2D culture.

Patsch et al. (2015) observed differentiation efficiencies between 61% and 88% for $CD144^{pos}$ cells in a 2D protocol. Certainly, such 2D differentiation protocols are generally scalable; however, scale-up of 2D differentiation culture with a total yield of 0.3×10^9 ECs for cellular therapy would require 17 T175 cell culture flasks with an average cell density of 1×10^5 cells/cm^2.

Applying our scalable 3D suspension culture protocol, we have now observed differentiation efficiencies of up to 76.8% $CD31^{pos}$ cells, which is similar to the 2D protocol reported by Patsch et al. (2015). Although the yield of 2.4 ECs per hiPSC is low compared with 25 ECs per hiPSC, which was achieved by Patsch et al., scalability of the established culture conditions allow to generate the same amount of ECs in agitated Erlenmeyer flasks with a total volume of 600 mL, e.g., in three 500-mL Erlenmeyer flasks with a working volume of 200 mL given the linear scalability of the used culture flask, as in 17 T175 flasks, without need for further *in vitro* expansion of the differentiated ECs. Feasibility of further scale-up could be shown by first experiments utilizing stirred-tank bioreactors. In addition to increased culture volumes these culture vessels also allow for detailed online process control and will allow GMP-compatible culture conditions, prerequisites for conceivable future clinical applications of hiPSC-derived ECs.

For molecular and functional assessment of hiPSC-derived ECs, it has to be considered that the EC lineage comprises different sublineages, including ECs of large

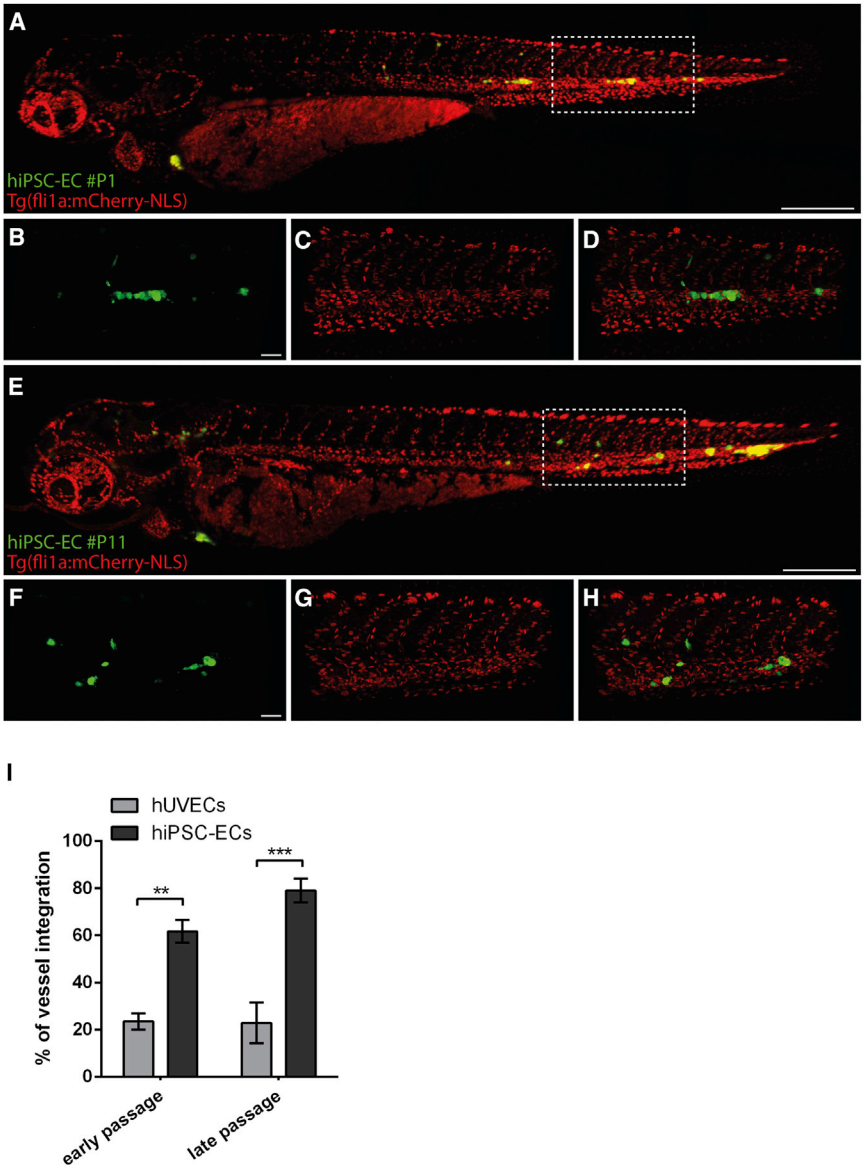

Figure 6. Vascular Competence of Early and Late hiPSC-Derived EC Passages in a Zebrafish Xenograft Model

Early (P1) passage hiPSC-ECs (green, hCBiPSCAGeGFP) within the embryonic zebrafish vasculature [marked by Tg(fli1a:mCherry-NLS)^{ubs10}, red)] 1 day after transplantation (A). Scale bar, 300 μm. Details of vessels with P1 hiPSC-EC (green) integration into the Tg(fli1a:mCherry-NLS)^{ubs10} transgenic embryonic zebrafish vasculature (red) (B–D). Scale bar, 50 μm. Late (P11) passage hiPSC-ECs (green) within the Tg(fli1a:mCherry-NLS)^{ubs10} transgenic embryonic zebrafish vasculature (red) 1 day after transplantation (E). Scale bar, 300 μm. Details of vessel with P11 hiPSC-EC (green) integration into the Tg(fli1a:mCherry-NLS)^{ubs10} transgenic embryonic zebrafish vasculature (red) (F–H). Scale bar, 50 μm. Quantification of integration rates of early and late hiPSC-ECs compared with early (P1, P4, and P5) and late (P14) hUVECs into the zebrafish embryonic vasculature 1 day after transplantation. Integration rates into the zebrafish vasculature were 61.9% (n = 83/134 embryos) for early hiPSC-ECs and 78.3% (n = 112/143 embryos) for late hiPSC-ECs. $^{**}p \leq 0.01$, $^{***}p \leq 0.001$ (I).

vessels and microvascular ECs, as well as arterial, venous, and lymphatic ECs. Such differences are of high relevance for modeling vascular diseases, since diseases such as artherosclerosis or pulmonary arterial hypertension do not affect arterial and venous vessels similarly. Likewise, success of drug development and cellular therapies will depend on ECs with suitable properties.

Although as yet not well understood, probably organ-specific differences exist and cultured proliferative ECs substantially differ from the normally quiescent ECs lining the vessel wall. It is still widely unknown to what extent the different types of ECs retain a memory due to their specific function (Gebb and Stevens, 2004) or possess sufficient plasticity to adopt the phenotype of other EC sublineages. Also, it is unclear whether embryonic and fetal ECs show a higher degree of plasticity than ECs in an adult individual.

As described recently (Orlova et al., 2014; Rufaihah et al., 2013), hPSC-derived ECs express both arterial and venous EC markers. We applied high concentrations of VEGFA as described by Patsch et al. (2015). Although it has to be considered that the biological activity of the VEGFA used in different studies (Orlova et al., 2014; Rufaihah et al., 2013) may have been different, and although we have applied even 4 times higher concentration of VEGFA than Rufaihah et al. (2013), our data generally confirm that treatment with high concentrations of VEGFA leads to a high expression of the arterial markers NRP1 and NOTCH1. In our hands, NRP1 and NOTCH1 expression

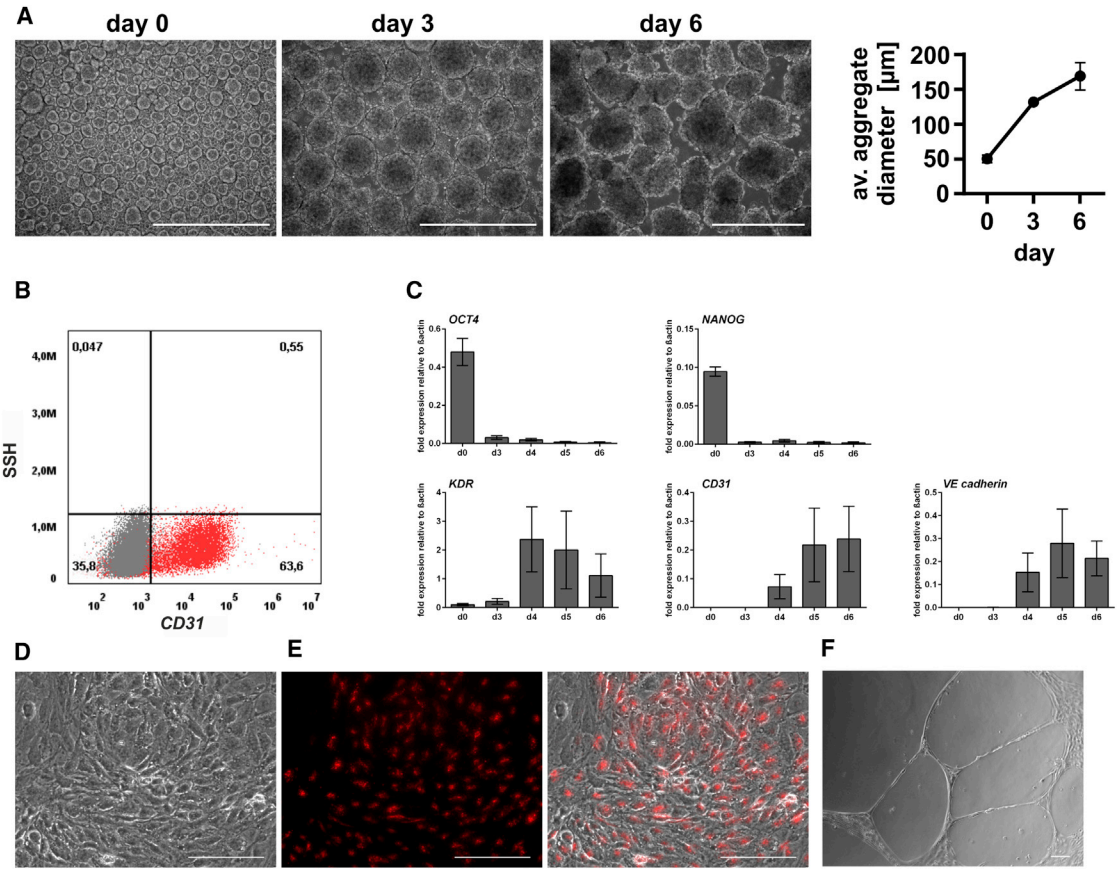

Figure 7. Scale-Up of EC Differentiation to Stirred-Tank Bioreactors

Single-cell-inoculated cultures (5 × 10^5 cells/mL, hCBiPs2CAGeGFP) formed aggregates with increasing diameter until day 6 of differentiation (A). Flow cytometric analysis showed robust generation of *CD31*^{pos} cells on day 6 of differentiation (56.8% ± 10.5%; n = 3 independent bioreactor runs, mean ± SEM, hCBiPS2CAGeGFP) representative plot (staining, red; isotype control, gray) (B). Gene expression analysis by quantitative real-time PCR showed downregulation of pluripotency-associated markers *OCT4* and *NANOG*, as well as upregulation of mesodermal marker (*KDR*) and endothelial cell markers (*VEcadherin*, *CD31*) (n = 3 independent bioreactor runs; mean ± SEM, hCBiPS2CAGeGFP) during differentiation (C). MACS-sorted *CD31*^{pos} hiPSC-ECs showed typical EC morphology in culture (D), uptake of Ac-Dil-LDL (E) after MACS separation and tube-forming assay demonstrated the angiogenic potential (F). Scale bars, 100 µm. See also Figure S4.

was even slightly higher than in cultured primary coronary aortic ECs (Figure 3E). Nevertheless, the venous markers EPHB4 and NRP2 were still expressed on a similar level as in hUVECs. Our findings that arterial and venous markers are simultaneously expressed on the protein level (Figure 3F) underline the not fully specified phenotype and a potential inherent plasticity of the generated ECs.

The functionality of the generated hiPSC-ECs was assessed applying four different assays. The classical tube-formation assay in Matrigel showed the angiogenic potential of the hiPSC-ECs, but, as it was shown that other non-ECs are also capable of network formation (Staton et al., 2009) and the hiPSC-EC networks showed less branching points compared with networks from hUVEC, we included additional assays. The ability to take up LDL represents another functional feature, also the antiviral response toward IAV was investigated in another approach.

Vascular endothelial cells can be infected by IAV and typically show an antiviral response indicated by upregulation of IFN-γ, CXCL10, and ISG15. It is noteworthy that vascular EC dysfunction is a hallmark of rare severe cases of IAV infection (reviewed in Armstrong et al., 2013), and patient-specific hiPSC-ECs should represent an excellent tool to further investigate genomic modifiers of this dysfunction. Our observations that the hiPSC-ECs showed characteristic IFN responses after infection with IAV, even with an IAV H1N1 field isolate showing a restriction of viral replication by host EC-derived IFITM3 protein (Sun et al., 2016), open the door for future detailed investigations of inter-individual differences in EC responses to

IAV infection, for instance for investigating IAV-EC interactions in individuals from different genetic backgrounds and in patients with different degrees of vasculopathy during IAV infection.

Furthermore, utilization of a zebrafish xenograft model showed functional properties of the generated hiPSC-ECs *in vivo*. Similar to findings described by Orlova et al. (2014), integration of hiPSC-derived ECs into the vasculature of zebrafish embryos might represent an *in vivo* model for human vascular diseases (Orlova et al., 2014). Moreover, as it was already shown for models of cancer and metastasis for drug discovery (Brown et al., 2017; Tat et al., 2013), the zebrafish model in combination with hiPSC-derived ECs might allow for investigation of specific disease underlying mutations *in vivo* and, more importantly, might represent a tool for drug discovery.

Since senescence is the main limiting factor for expansion of primary ECs, and the related loss of marker expression and functionality in late passages is a well-known phenomenon (Unterluggauer et al., 2007), we investigated the expansion rate during culture and a potential loss of functionality in iPSC-ECs after extended propagation. During culture expansion, the population doubling time remained almost constant, e.g., 1.6 days in passage 2 and 1.3 days in passage 8. Remarkably, we could not detect any loss of functionality at passage 12 in terms of vascular network formation or uptake of Ac-LDL. In addition, no significant differences were observed in integration efficiency of early and late passage hiPSC-ECs in the zebrafish xenograft model, also underlining the stable phenotype of the generated and expanded hiPSC-ECs.

As extended culture of primary human ECs has also been shown to be accompanied with the appearance of chromosomal abnormalities (Corselli et al., 2008; Johnson et al., 1992; Nichols et al., 1987), we also investigated the maintenance of genetic integrity during and after extended propagation of hiPSC-ECs.

Most karyotypic abnormalities in EC expansion cultures arise due to telomere erosion, which could be detected in ECs isolated from patients with, e.g., coronary artery disease (Ogami et al., 2004), but also ECs from healthy donors showed a decline of telomere length with increasing age (Chang and Harley, 1995). Telomere shortening can initiate repeated breakage-fusion-bridge cycles leading to chromosomal instability (Begus-Nahrmann et al., 2012), chromosome rearrangements (Artandi et al., 2000), aneuploidies (Pampalona et al., 2010), and polyploidies (Pampalona et al., 2012), and typically leads to senescence, apoptosis, but in some cases also cancer formation. Since reprogramming restores elongation of telomeres (Agarwal et al., 2010), we hypothesized that the risk of karyotypic changes due to telomere erosion is reduced in ECs derived from karyotypically normal hiPSCs compared with primary ECs.

Consistent with published data (Corselli et al., 2008), we detected chromosomal aberrations in all tested hUVEC and hCBEC isolations after prolonged *in vitro* culture (>11 passages). A loss of chromosome 13 was already observed in hCBECs in passage 5 and may have occurred independently of telomere erosion as previously suggested (Kimura et al., 2004; Zhang et al., 2000). Besides that, chromosomal aberrations could be detected also in *in vitro* expanded adult ECs (hPBECs and hSVECs) in up to 60% of the analyzed metaphases already at passage 5–6.

As hypothesized, the hiPSC-derived ECs showed a much higher chromosomal stability with an intact karyotype in 98% of the analyzed metaphases under similar culture conditions as the primary ECs.

Conclusion

The scalable protocol described here offers for the first time the opportunity to generate large numbers of (patient-specific) ECs which show a lower rate of chromosomal abnormalities or phenotypical alterations than primary cells after *in vitro* expansion. Moreover, utilizing controllable mass expansion of undifferentiated hiPSC allows generation of large hiPSC-EC numbers even without additional culture, avoiding or minimizing the risk for chromosomal aberrations or phenotypical changes after prolonged *in vitro* culture. Functional tests showed the applicability of the generated ECs for *in vitro* assays to investigate angiogenesis or cellular responses to viral infections. Furthermore, the opportunity to generate patient-specific ECs in relevant numbers for cell therapy approaches, even from adult patients, might also allow to utilize these hiPSC-ECs in regenerative approaches.

EXPERIMENTAL PROCEDURES

Human material was collected after approval by the local Ethics Committee and following the donor's written informed consent, or in the case of newborns, following parental consent. Handling of zebrafish was done in compliance with German and Lower Saxony state law, carefully monitored by the local authority for animal protection (LAVES, Lower Saxony, Germany; Animal protocol. 42500/1H).

Differentiation

To induce EC differentiation, hiPSC cultures hCBiPS2 (Haase et al., 2009), hCBiPS2CAGeGFP (Merkert et al., 2014), hHSC1285iPS2 (https://hpscreg.eu, MHHi006-A [Hartung et al., 2013]), and hHSCSeViPS2 (https://hpscreg.eu, MHHi001-A [Kempf et al., 2016]) were treated on day 0 with 25 ng/mL BMP4 (Bio-Techne, Minneapolis, USA) and the WNT pathway activator CHIR 90221 (7.5 μM) in N2B27 medium (Thermo Fischer Scientific, Waltham, MA, USA) for 2 days without any medium exchange. From days 3 to 7, cultures were maintained in StemPro-34 medium (Thermo Fischer Scientific) supplemented with 260 ng/mL rhVEGFA$_{165}$

and 2 μM forskolin (Sigma-Aldrich, St. Louis, USA) with daily medium exchanges.

Bioreactor Differentiation

Stirred DASbox mini-bioreactors (DASGIP/Eppendorf) were prepared as described previously (Kempf et al., 2014; Olmer et al., 2012). Cultures were inoculated with 5×10^5 cells/mL in the final 120 mL culture volume.

Aggregate samples were monitored by light microscopy; images were captured (Axio Vert.A1; Zeiss) and processed in AxioVision (Zeiss) to define diameter and size distribution. Mean diameters represent the arithmetic average of >25 independent aggregates.

SUPPLEMENTAL INFORMATION

Supplemental Information includes Supplemental Experimental Procedures, five figures, and two tables and can be found with this article online at https://doi.org/10.1016/j.stemcr.2018.03.017.

AUTHOR CONTRIBUTIONS

R.O. conceived and designed the study, collected and assembled the data, performed data analysis and interpretation, and wrote the paper. L.E., H.K., R.Z., D.B., and S.A.-S. collected the data and performed data analysis and interpretation. A.U., S.M., and M.N.H.M. collected the data. F.P. performed data analysis and interpretation. T.S. and S.B. provided the study material. G.G. provided analytical technologies and collected the data. U.M. conceived and designed the study, performed data analysis and interpretation, and wrote the paper.

ACKNOWLEDGMENTS

We thank Dr. A. Haase for providing hiPSCs, Dr K. Osetek for isolation of hUVEC as well as hCBECs, and M. Szepes for performing tube-forming assay of hUVECs. We thank M. Lönne and A. Franke for technical assistance. This work was funded by the German Research Foundation (KFO311, MA 2331/18-1; MA 2331/15-1, SFB958, SE2016/7-2, SE2016/10-1, ZW64/4-1, and KFO311-ZW64/7-1), the German Center for Lung Research (DZL, BREATH 82DZL002A1), and the German Research Foundation (Cluster of Excellence REBIRTH, EXC 62), by the German Ministry for Education and Science (BMBF, grants: 13N14086, 01EK1601A, and 01EK1602A), by the European Union (TECHNOBEAT, grant 668724), and by StemBANCC (receiving support from the Innovative Medicines Initiative joint undertaking under grant 115439-2, whose resources are composed of financial contribution from the European Union [FP7/2007-2013] and EFPIA companies' in-kind contribution).

Received: October 23, 2017
Revised: March 20, 2018
Accepted: March 20, 2018
Published: April 19, 2018

REFERENCES

Agarwal, S., Loh, Y.H., McLoughlin, E.M., Huang, J., Park, I.H., Miller, J.D., Huo, H., Okuka, M., Dos Reis, R.M., Loewer, S., et al. (2010). Telomere elongation in induced pluripotent stem cells from dyskeratosis congenita patients. Nature *464*, 292–296.

Albertson, D.G., Collins, C., McCormick, F., and Gray, J.W. (2003). Chromosome aberrations in solid tumors. Nat. Genet. *34*, 369–376.

Andrée, B., Bela, K., Horvath, T., Lux, M., Ramm, R., Venturini, L., Ciubotaru, A., Zweigerdt, R., Haverich, A., and Hilfiker, A. (2014). Successful re-endothelialization of a perfusable biological vascularized matrix (BioVaM) for the generation of 3D artificial cardiac tissue. Basic Res. Cardiol. *109*, 441.

Armstrong, S.M., Darwish, I., and Lee, W.L. (2013). Endothelial activation and dysfunction in the pathogenesis of influenza A virus infection. Virulence *4*, 537–542.

Artandi, S.E., Chang, S., Lee, S.L., Alson, S., Gottlieb, G.J., Chin, L., and DePinho, R.A. (2000). Telomere dysfunction promotes nonreciprocal translocations and epithelial cancers in mice. Nature *406*, 641–645.

Asahara, T., Kawamoto, A., and Masuda, H. (2011). Concise review: circulating endothelial progenitor cells for vascular medicine. Stem Cells *29*, 1650–1655.

Begus-Nahrmann, Y., Hartmann, D., Kraus, J., Eshraghi, P., Scheffold, A., Grieb, M., Rasche, V., Schirmacher, P., Lee, H.W., Kestler, H.A., et al. (2012). Transient telomere dysfunction induces chromosomal instability and promotes carcinogenesis. J. Clin. Invest. *122*, 2283–2288.

Boerma, M., Burton, G.R., Wang, J., Fink, L.M., McGehee, R.E., Jr., and Hauer-Jensen, M. (2006). Comparative expression profiling in primary and immortalized endothelial cells: changes in gene expression in response to hydroxy methylglutaryl-coenzyme A reductase inhibition. Blood Coagul. Fibrinolysis *17*, 173–180.

Bou Khzam, L., Bouchereau, O., Boulahya, R., Hachem, A., Zaid, Y., Abou-Saleh, H., and Merhi, Y. (2015). Early outgrowth cells versus endothelial colony forming cells functions in platelet aggregation. J. Transl. Med. *13*, 353.

Brown, H.K., Schiavone, K., Tazzyman, S., Heymann, D., and Chico, T.J. (2017). Zebrafish xenograft models of cancer and metastasis for drug discovery. Expert Opin. Drug Discov. *12*, 379–389.

Cebotari, S., Tudorache, I., Ciubotaru, A., Boethig, D., Sarikouch, S., Goerler, A., Lichtenberg, A., Cheptanaru, E., Barnaciuc, S., Cazacu, A., et al. (2011). Use of fresh decellularized allografts for pulmonary valve replacement may reduce the reoperation rate in children and young adults: early report. Circulation *124*, S115–S123.

Chang, E., and Harley, C.B. (1995). Telomere length and replicative aging in human vascular tissues. Proc. Natl. Acad. Sci. USA *92*, 11190–11194.

Chong, M.S., Ng, W.K., and Chan, J.K. (2016). Concise review: endothelial progenitor cells in regenerative medicine: applications and challenges. Stem Cells Transl. Med. *5*, 530–538.

Colombo, E., Calcaterra, F., Cappelletti, M., Mavilio, D., and Della Bella, S. (2013). Comparison of fibronectin and collagen in supporting the isolation and expansion of endothelial progenitor cells from human adult peripheral blood. PLoS One *8*, e66734.

Corselli, M., Parodi, A., Mogni, M., Sessarego, N., Kunkl, A., Dagna-Bricarelli, F., Ibatici, A., Pozzi, S., Bacigalupo, A., Frassoni, F., et al.

(2008). Clinical scale ex vivo expansion of cord blood-derived outgrowth endothelial progenitor cells is associated with high incidence of karyotype aberrations. Exp. Hematol. *36*, 340–349.

Cucullo, L., Couraud, P.O., Weksler, B., Romero, I.A., Hossain, M., Rapp, E., and Janigro, D. (2008). Immortalized human brain endothelial cells and flow-based vascular modeling: a marriage of convenience for rational neurovascular studies. J. Cereb. Blood Flow Metab. *28*, 312–328.

Daniels, B.P., Cruz-Orengo, L., Pasieka, T.J., Couraud, P.O., Romero, I.A., Weksler, B., Cooper, J.A., Doering, T.L., and Klein, R.S. (2013). Immortalized human cerebral microvascular endothelial cells maintain the properties of primary cells in an in vitro model of immune migration across the blood brain barrier. J. Neurosci. Methods *212*, 173–179.

Esper, R.J., Nordaby, R.A., Vilariño, J.O., Paragano, A., Cacharrón, J.L., and Machado, R.A. (2006). Endothelial dysfunction: a comprehensive appraisal. Cardiovasc. Diabetol. *5*, 4.

Farcas, M.A., Rouleau, L., Fraser, R., and Leask, R.L. (2009). The development of 3-D, in vitro, endothelial culture models for the study of coronary artery disease. Biomed. Eng. Online *8*, 30.

Franck, G., Dai, J., Fifre, A., Ngo, S., Justine, C., Michineau, S., Allaire, E., and Gervais, M. (2013). Reestablishment of the endothelial lining by endothelial cell therapy stabilizes experimental abdominal aortic aneurysms. Circulation *127*, 1877–1887.

Gebb, S., and Stevens, T. (2004). On lung endothelial cell heterogeneity. Microvasc. Res. *68*, 1–12.

Goya, K., Otsuki, M., Xu, X., and Kasayama, S. (2003). Effects of the prostaglandin I2 analogue, beraprost sodium, on vascular cell adhesion molecule-1 expression in human vascular endothelial cells and circulating vascular cell adhesion molecule-1 level in patients with type 2 diabetes mellitus. Metabolism *52*, 192–198.

Gruh, I., Beilner, J., Blomer, U., Schmiedl, A., Schmidt-Richter, I., Kruse, M.L., Haverich, A., and Martin, U. (2006). No evidence of transdifferentiation of human endothelial progenitor cells into cardiomyocytes after coculture with neonatal rat cardiomyocytes. Circulation *113*, 1326–1334.

Haase, A., Olmer, R., Schwanke, K., Wunderlich, S., Merkert, S., Hess, C., Zweigerdt, R., Gruh, I., Meyer, J., Wagner, S., et al. (2009). Generation of induced pluripotent stem cells from human cord blood. Cell Stem Cell *5*, 434–441.

Haldi, M., Ton, C., Seng, W.L., and McGrath, P. (2006). Human melanoma cells transplanted into zebrafish proliferate, migrate, produce melanin, form masses and stimulate angiogenesis in zebrafish. Angiogenesis *9*, 139–151.

Hartung, S., Schwanke, K., Haase, A., David, R., Franz, W.M., Martin, U., and Zweigerdt, R. (2013). Directing cardiomyogenic differentiation of human pluripotent stem cells by plasmid-based transient overexpression of cardiac transcription factors. Stem Cells Dev. *22*, 1112–1125.

Heiss, M., Hellstrom, M., Kalen, M., May, T., Weber, H., Hecker, M., Augustin, H.G., and Korff, T. (2015). Endothelial cell spheroids as a versatile tool to study angiogenesis in vitro. FASEB J. *29*, 3076–3084.

Hess, C., Wiegmann, B., Maurer, A.N., Fischer, P., Möller, L., Martin, U., Hilfiker, A., Haverich, A., and Fischer, S. (2010). Reduced thrombocyte adhesion to endothelialized poly 4-methyl-1-pentene gas exchange membranes - a first step toward bioartificial lung development. Tissue Eng. Part A *16*, 3043–3053.

Hiyoshi, M., Indalao, I.L., Yano, M., Yamane, K., Takahashi, E., and Kido, H. (2015). Influenza A virus infection of vascular endothelial cells induces GSK-3beta-mediated beta-catenin degradation in adherens junctions, with a resultant increase in membrane permeability. Arch. Virol. *160*, 225–234.

Igreja, C., Fragoso, R., Caiado, F., Clode, N., Henriques, A., Camargo, L., Reis, E.M., and Dias, S. (2008). Detailed molecular characterization of cord blood-derived endothelial progenitors. Exp. Hematol. *36*, 193–203.

Ikuno, T., Masumoto, H., Yamamizu, K., Yoshioka, M., Minakata, K., Ikeda, T., Sakata, R., and Yamashita, J.K. (2017). Efficient and robust differentiation of endothelial cells from human induced pluripotent stem cells via lineage control with VEGF and cyclic AMP. PLoS One *12*, e0173271.

Johnson, T.E., Umbenhauer, D.R., Hill, R., Bradt, C., Mueller, S.N., Levine, E.M., and Nichols, W.W. (1992). Karyotypic and phenotypic changes during in vitro aging of human endothelial cells. J. Cell. Physiol. *150*, 17–27.

Kang, H.W., Walvick, R., and Bogdanov, A., Jr. (2009). In vitro and in vivo imaging of antivasculogenesis induced by Noggin protein expression in human venous endothelial cells. FASEB J. *23*, 4126–4134.

Kempf, H., Olmer, R., Kropp, C., Ruckert, M., Jara-Avaca, M., Robles-Diaz, D., Franke, A., Elliott, D.A., Wojciechowski, D., Fischer, M., et al. (2014). Controlling expansion and cardiomyogenic differentiation of human pluripotent stem cells in scalable suspension culture. Stem Cell Reports *3*, 1132–1146.

Kempf, H., Kropp, C., Olmer, R., Martin, U., and Zweigerdt, R. (2015). Cardiac differentiation of human pluripotent stem cells in scalable suspension culture. Nat. Protoc. *10*, 1345–1361.

Kempf, H., Olmer, R., Haase, A., Franke, A., Bolesani, E., Schwanke, K., Robles-Diaz, D., Coffee, M., Göhring, G., Dräger, G., et al. (2016). Bulk cell density and Wnt/TGFbeta signalling regulate mesendodermal patterning of human pluripotent stem cells. Nat. Commun. *7*, 13602.

Kim, S., and von Recum, H. (2008). Endothelial stem cells and precursors for tissue engineering: cell source, differentiation, selection, and application. Tissue Eng. Part B Rev. *14*, 133–147.

Kimura, A., Ohmichi, M., Kawagoe, J., Kyo, S., Mabuchi, S., Takahashi, T., Ohshima, C., Arimoto-Ishida, E., Nishio, Y., Inoue, M., et al. (2004). Induction of hTERT expression and phosphorylation by estrogen via Akt cascade in human ovarian cancer cell lines. Oncogene *23*, 4505–4515.

Kropp, C., Kempf, H., Halloin, C., Robles-Diaz, D., Franke, A., Scheper, T., Kinast, K., Knorpp, T., Joos, T.O., Haverich, A., et al. (2016). Impact of feeding strategies on the scalable expansion of human pluripotent stem cells in single-use stirred tank bioreactors. Stem Cells Transl. Med. *5*, 1289–1301.

L'Heureux, N., Dusserre, N., Konig, G., Victor, B., Keire, P., Wight, T.N., Chronos, N.A., Kyles, A.E., Gregory, C.R., Hoyt, G., et al. (2006). Human tissue-engineered blood vessels for adult arterial revascularization. Nat. Med. *12*, 361–365.

Levenberg, S., Golub, J.S., Amit, M., Itskovitz-Eldor, J., and Langer, R. (2002). Endothelial cells derived from human embryonic stem cells. Proc. Natl. Acad. Sci. USA *99*, 4391–4396.

Lian, X., Bao, X., Al-Ahmad, A., Liu, J., Wu, Y., Dong, W., Dunn, K.K., Shusta, E.V., and Palecek, S.P. (2014). Efficient differentiation of human pluripotent stem cells to endothelial progenitors via small-molecule activation of WNT signaling. Stem Cell Reports *3*, 804–816.

Liu, X., Qi, J., Xu, X., Zeisberg, M., Guan, K., and Zeisberg, E.M. (2016). Differentiation of functional endothelial cells from human induced pluripotent stem cells: a novel, highly efficient and cost effective method. Differentiation *92*, 225–236.

Mayshar, Y., Ben-David, U., Lavon, N., Biancotti, J.C., Yakir, B., Clark, A.T., Plath, K., Lowry, W.E., and Benvenisty, N. (2010). Identification and classification of chromosomal aberrations in human induced pluripotent stem cells. Cell Stem Cell *7*, 521–531.

Merkert, S., Wunderlich, S., Bednarski, C., Beier, J., Haase, A., Dreyer, A.K., Schwanke, K., Meyer, J., Gohring, G., Cathomen, T., et al. (2014). Efficient designer nuclease-based homologous recombination enables direct PCR screening for footprintless targeted human pluripotent stem cells. Stem Cell Reports *2*, 107–118.

Michiels, C. (2003). Endothelial cell functions. J. Cell. Physiol. *196*, 430–443.

Mohan, C.C., Chennazhi, K.P., and Menon, D. (2013). In vitro hemocompatibility and vascular endothelial cell functionality on titania nanostructures under static and dynamic conditions for improved coronary stenting applications. Acta Biomater. *9*, 9568–9577.

Nichols, W.W., Buynak, E.B., Bradt, C., Hill, R., Aronson, M., Jarrell, B.E., Mueller, S.N., and Levine, E.M. (1987). Cytogenetic evaluation of human endothelial cell cultures. J. Cell. Physiol. *132*, 453–462.

Ogami, M., Ikura, Y., Ohsawa, M., Matsuo, T., Kayo, S., Yoshimi, N., Hai, E., Shirai, N., Ehara, S., Komatsu, R., et al. (2004). Telomere shortening in human coronary artery diseases. Arterioscler. Thromb. Vasc. Biol. *24*, 546–550.

Olmer, R., Lange, A., Selzer, S., Kasper, C., Haverich, A., Martin, U., and Zweigerdt, R. (2012). Suspension culture of human pluripotent stem cells in controlled, stirred bioreactors. Tissue Eng. Part C Methods *18*, 772–784.

Orlova, V.V., Drabsch, Y., Freund, C., Petrus-Reurer, S., van den Hil, F.E., Muenthaisong, S., Dijke, P.T., and Mummery, C.L. (2014). Functionality of endothelial cells and pericytes from human pluripotent stem cells demonstrated in cultured vascular plexus and zebrafish xenografts. Arterioscler. Thromb. Vasc. Biol. *34*, 177–186.

Pampalona, J., Soler, D., Genesca, A., and Tusell, L. (2010). Whole chromosome loss is promoted by telomere dysfunction in primary cells. Genes Chromosomes Cancer *49*, 368–378.

Pampalona, J., Frias, C., Genesca, A., and Tusell, L. (2012). Progressive telomere dysfunction causes cytokinesis failure and leads to the accumulation of polyploid cells. PLoS Genet. *8*, e1002679.

Patsch, C., Challet-Meylan, L., Thoma, E.C., Urich, E., Heckel, T., O'Sullivan, J.F., Grainger, S.J., Kapp, F.G., Sun, L., Christensen, K., et al. (2015). Generation of vascular endothelial and smooth muscle cells from human pluripotent stem cells. Nat. Cell Biol. *17*, 994–1003.

Reed, D.M., Foldes, G., Harding, S.E., and Mitchell, J.A. (2013). Stem cell-derived endothelial cells for cardiovascular disease: a therapeutic perspective. Br. J. Clin. Pharmacol. *75*, 897–906.

Rohde, E., Malischnik, C., Thaler, D., Maierhofer, T., Linkesch, W., Lanzer, G., Guelly, C., and Strunk, D. (2006). Blood monocytes mimic endothelial progenitor cells. Stem Cells *24*, 357–367.

Rufaihah, A.J., Huang, N.F., Jamé, S., Lee, J.C., Nguyen, H.N., Byers, B., De, A., Okogbaa, J., Rollins, M., Reijo-Pera, R., et al. (2011). Endothelial cells derived from human iPSCS increase capillary density and improve perfusion in a mouse model of peripheral arterial disease. Arterioscler. Thromb. Vasc. Biol. *31*, e72–e79.

Rufaihah, A.J., Huang, N.F., Kim, J., Herold, J., Volz, K.S., Park, T.S., Lee, J.C., Zambidis, E.T., Reijo-Pera, R., and Cooke, J.P. (2013). Human induced pluripotent stem cell-derived endothelial cells exhibit functional heterogeneity. Am. J. Transl. Res. *5*, 21–35.

Sakao, S., Tatsumi, K., and Voelkel, N.F. (2009). Endothelial cells and pulmonary arterial hypertension: apoptosis, proliferation, interaction and transdifferentiation. Respir. Res. *10*, 95.

Shao, R., and Guo, X. (2004). Human microvascular endothelial cells immortalized with human telomerase catalytic protein: a model for the study of in vitro angiogenesis. Biochem. Biophys. Res. Commun. *321*, 788–794.

Short, K.R., Veldhuis Kroeze, E.J., Reperant, L.A., Richard, M., and Kuiken, T. (2014). Influenza virus and endothelial cells: a species specific relationship. Front. Microbiol. *5*, 653.

Shuga, J., Zeng, Y., Novak, R., Mathies, R.A., Hainaut, P., and Smith, M.T. (2010). Selected technologies for measuring acquired genetic damage in humans. Environ. Mol. Mutagen. *51*, 851–870.

Skovseth, D.K., Yamanaka, T., Brandtzaeg, P., Butcher, E.C., and Haraldsen, G. (2002). Vascular morphogenesis and differentiation after adoptive transfer of human endothelial cells to immunodeficient mice. Am. J. Pathol. *160*, 1629–1637.

Staton, C.A., Reed, M.W., and Brown, N.J. (2009). A critical analysis of current in vitro and in vivo angiogenesis assays. Int. J. Exp. Pathol. *90*, 195–221.

Sun, X., Belser, J.A., Pulit-Penaloza, J.A., Zeng, H., Lewis, A., Shieh, W.J., Tumpey, T.M., and Maines, T.R. (2016). Pathogenesis and transmission assessments of two H7N8 influenza A viruses recently isolated from Turkey farms in Indiana using mouse and ferret models. J. Virol. *90*, 10936–10944.

Tan, J.Y., Sriram, G., Rufaihah, A.J., Neoh, K.G., and Cao, T. (2013). Efficient derivation of lateral plate and paraxial mesoderm subtypes from human embryonic stem cells through GSKi-mediated differentiation. Stem Cells Dev. *22*, 1893–1906.

Tang, Z.C., Liao, W.Y., Tang, A.C., Tsai, S.J., and Hsieh, P.C. (2011). The enhancement of endothelial cell therapy for angiogenesis in hindlimb ischemia using hyaluronan. Biomaterials *32*, 75–86.

Tat, J., Liu, M., and Wen, X.Y. (2013). Zebrafish cancer and metastasis models for in vivo drug discovery. Drug Discov. Today Technol. *10*, e83–e89.

Theodoridis, K., Tudorache, I., Calistru, A., Cebotari, S., Meyer, T., Sarikouch, S., Bara, C., Brehm, R., Haverich, A., and Hilfiker, A. (2015). Successful matrix guided tissue regeneration of

decellularized pulmonary heart valve allografts in elderly sheep. Biomaterials *52*, 221–228.

Unterluggauer, H., Hütter, E., Voglauer, R., Grillari, J., Vöth, M., Bereiter-Hahn, J., Jansen-Dürr, P., and Jendrach, M. (2007). Identification of cultivation-independent markers of human endothelial cell senescence in vitro. Biogerontology *8*, 383–397.

Yamamizu, K., and Yamashita, J.K. (2011). Roles of cyclic adenosine monophosphate signaling in endothelial cell differentiation and arterial-venous specification during vascular development. Circ. J. *75*, 253–260.

Yang, L., Soonpaa, M.H., Adler, E.D., Roepke, T.K., Kattman, S.J., Kennedy, M., Henckaerts, E., Bonham, K., Abbott, G.W., Linden, R.M., et al. (2008). Human cardiovascular progenitor cells develop from a KDR+ embryonic-stem-cell-derived population. Nature *453*, 524–528.

Zhang, A., Zheng, C., Lindvall, C., Hou, M., Ekedahl, J., Lewensohn, R., Yan, Z., Yang, X., Henriksson, M., Blennow, E., et al. (2000). Frequent amplification of the telomerase reverse transcriptase gene in human tumors. Cancer Res. *60*, 6230–6235.

Zhang, S.J., Zhang, H., Wei, Y.J., Su, W.J., Liao, Z.K., Hou, M., Zhou, J.Y., and Hu, S.S. (2006). Adult endothelial progenitor cells from human peripheral blood maintain monocyte/macrophage function throughout in vitro culture. Cell Res. *16*, 577–584.